Title	Charge resolved electrostatic diagnostic of colliding copper laser plasma plumes
Authors(s)	Yeates, P; Fallon, Conor; Kennedy, E.T.; Costello, John T.
Publication date	2011
Publication information	Physics of Plasmas, 18 (10): 103104-1-103114-10
Publisher	American Institute of Physics
Item record/more information	http://hdl.handle.net/10197/3614
Publisher's statement	The following article appeared in Physics of Plasmas 18, 103104 (2011), DOI:10.1063/1.3633486 and may be found at http://dx.doi.org/10.1063/1.3633486. The article may be downloaded for personal use only. Any other use requires prior permission of the author and the American Institute of Physics.
Publisher's version (DOI)	10.1063/1.3633486

Charge Resolved Electrostatic Diagnostic of Colliding Copper Laser Plasma Plumes.

[1]P. Yeates, [2]C. Fallon, [1, 2]E. T. Kennedy, [1, 2]J. T. Costello

[1]National Centre for Plasma Science and Technology (NCPST), Dublin City University (DCU), Ireland.

[2]School of Physical Sciences, Dublin City University (DCU), Dublin, Ireland.

Abstract

The collision of two laser generated plasma plumes can result, under appropriate conditions, in the formation of a '*stagnation layer*'. The processes underlying this phenomenon are complex and time dependent. The majority of experiments over the last few decades have focused upon spectroscopic diagnostic of colliding plasmas. We have performed electrostatic diagnosis of multiply charged copper ions (Cu^{+} to Cu^{5+}) generated *via* Q-switched pulsed laser (λ=1.06 μm, τ=6 ns, E_L=52-525 mJ) generation of copper plasma plumes from a planar target. Time dependent current traces, charge yields and kinetic energy (K_e) distributions are obtained for single plasma plumes (S_p) and colliding plasma plumes (C_p). The charge yield from a C_p relative to twice that from a S_p is characterized by a charge yield ratio *(CYR)* parameter. Superior ion yields for all charge states occur for a discrete range of fluences (F) from colliding plasma plumes leading to a *CYR* parameter exceeding unity. The kinetic energy distributions from colliding plasma plumes display well defined energy compression *via* narrowing of the distributions for all fluences and charge states. The extent of this energy compression is charge dependent. Space charge forces within the stagnation layer and

the resulting charge dependent acceleration of ions is proposed to account for the transfer of ion kinetic energy in favour of collisional ionization mechanisms.

Keywords: Copper colliding plasma, diagnostic, Faraday cup, gridded retarding field analyzer, charge resolved, charge yield, energy compression.

I. INTRODUCTION

The study of colliding plasma plumes has been ongoing since the early sixties[1-6]. For high intensity laser plasma generation (I_p>10^{13} Wcm^{-2}) the experimental focus was motivated by inertial confinement fusion studies (ICF)[7-10]. Early investigations attempted to identify the complex mechanisms responsible for the formation of a unique phenomenon later termed[5] a '*stagnation layer*'. The collision and interpenetration of two laser plasma plumes is an extremely complex time dependent process and has yet to be fully elucidated.

The observed dynamics of such a system were initially reported to depend heavily upon the initial electron density (N_{eo}) of the seed plasmas and also on their spatial separation[6]. Where the mean free path (*mfp*) was sufficiently small, a 'cold' electron layer would form in the interaction zone where the two seed plumes interact[5]. This highly localized region exhibited a jump in the local electron density (N_e) by a factor of ~5 in comparison to the seed plasmas[5].

This aspect of stagnation layer formation originates in the highly collisional interaction of 'fast' electrons (electron *mfp*, λ_{ee}~2 μm)[6] which precede the ions. Ions

enter this interaction zone and subsequent ion-ion collisions heat this zone appreciably (T_e/T_{ion}~1→8 over the interaction timescale), provided that the electron density, N_e is high enough.

Interest in colliding laser plasma plumes (CLPP) and their possible applications have also resulted in a range of experiments attempting to modify the quality of thin film deposition[11-14] for a range of materials. In contrast spectroscopic investigations of colliding laser plasma plumes have concentrated on short wavelength studies i.e. vacuum ultraviolet (VUV)[15], extreme ultraviolet (EUV) and x-ray spectral ranges[16-26]. Attempts have also been made to simulate colliding laser plasma plumes for comparison with experimental results[21,26- 28].

More recently a large number of experiments in the visible spectral range, augmented by high speed imaging of CLPP have been reported[29-33] and target geometries utilized were either planar or wedge (varying angle) with plasma plumes streaming laterally or transversely. To date there have been very few reports on electrostatic diagnostic of CLPP[34,35] and no charge resolved electrostatic studies have yet been reported.

In this report we present charged resolved measurements of Cu^+ to Cu^{5+} ions from single (S_p) and colliding (C_p) copper laser plasma plumes generated *via* Q-switched laser pulse ablation of a planar target. A gridded retarding field analyzer (RFA) combined with a Faraday cup detector is utilized to detect plasma ion time-of-flight (*TOF*) signals after the ions have traversed a drift tube (d=1.13 m). For a range of fluences (F=0.08-0.84 Jcm^{-2}), we use deconvoluted, time dependent current traces

to determine the dependence of the charge-resolved ion yield on laser fluence (F). We introduce a parameter that we term the 'charge yield ratio' *(CYR)* to quantify the gain (or loss) in charge yield for colliding plasmas over single plasma plumes. We also convert the current traces to kinetic energy (K_e) distributions to reveal a strong narrowing of the kinetic energy distribution in the C_p in concert with a lowering of the recorded peak K_e. This aspect of C_p is observed to be strongly charge dependent.

II. Colliding Plasma Fundamentals

As previously stated, the magnitude of various processes responsible for stagnation layer formation are strongly dependent upon the incident N_e at the collision front and also on the edge velocity of the plasma plume. Two regimes have been identified. *Soft* stagnation occurs where there is a small degree of interpenetration between the two counter-streaming seed plasma plumes. In this case the ion-ion mean-free-path (*mfp*) is generally larger than the dimensions of the system[27] i.e. the separation of the seed plasmas. The primary heating process in this case originates in the ionic collisions within each individual seed plasma. Relative velocities of the seed plumes are usually high.

In contrast, *hard* stagnation occurs when the ion-ion *mfp* is less than the seed separation, D. The two plasmas undergo rapid deceleration and little or no interpenetration occurs. Collisions between ions from opposing plumes dominate, resulting in the conversion of plasma kinetic energy which generates highly localized heating at the collision front. The rapid build up of plasma at this point results in the

formation of a dense layer of material termed the *stagnation layer* and heating of this layer produces bright emission.

The collisionality parameter[23,27,30] ξ - determines which collision scenario will occur and is given by[23].

$$\xi = D/\lambda_{ii} \qquad \text{Eq. 1}$$

Where D is the separation between the two seed plasma plumes and λ_{ii} is the ion-ion mean free path given by[23,30]:

$$\lambda_{ii}(1 \rightarrow 2) = \frac{4\pi\varepsilon_0^2 m^2 v_{12}^4}{e^4 z^4 N_i \ln \Lambda_{1\rightarrow 2}} \qquad \text{Eq. 2}$$

N_i is the plasma average ion density at the point of collision, v_{12} is the relative collision velocity, z is the average ionization state of the plasma, m the mass of the atom (kg) and ε_0 is the permittivity of free space (8.85×10^{-12} m^{-3} kg^{-1} s^4 A^2). $\ln\Lambda_{1\rightarrow 2}$ is the so-called Coulomb logarithm.

High values of the collisionality parameter (ξ) can be achieved if the seed plasma plumes are generated close together but exhibit small ion-ion *mfp*, λ_{ii}. Given that $\lambda_{ii} \propto T^2/N_i$ (N_i = ion density)[33], seed plasma plumes with low temperature and high density will lead to tight stagnation layer formation. A simple calculation for a hydrogen like plasma with T~1.4 eV and N_i~10^{18} cm^{-3} results in a collisionality parameter value[33] of ξ~10^4.

III. EXPERIMENTIAL SETUP

A. Plasma generation

Laser plasmas were reproducibly created with Nd:yttrium aluminum garnet Q-switched laser pulses (λ=1.06 μm, τ=6 ns, and E_L=0.5-0.52 mJ). Generation of the two seed plasmas was achieved with the aid of a wedge prism which splits the incoming single laser pulse (before focusing) into two separate beams. Focused beams were achieved *via* a 28 cm convex-planar lens. The laser irradiance was varied from I_P=0.13-1.4×10^{11} Wcm^{-2} with a ϕ=200 μm spot size for each individual plasma. Single plasma generation was achieved by blocking one of the split beams before the focusing lens.

The separation of the two focused beams (in mm) in the plane of the target is given by[30]:

$$D = \gamma f(n-1) \qquad \text{Eq. 3}$$

where γ is the wedge angle in radians and f is the focal length of the lens in millimetres. n is the refractive index of the lens material (n=1.5). The distance between the wedge prism and focusing lens was varied in order to ensure that the seed plasma separation D was ~2.5 mm. Operating pressures of ~3×10^{-6} mbar were maintained for all experiments.

Figure 1(a) and (b) display a schematic of the vacuum chamber and optical-beam/plasma configuration. Figure 1(c) displays typical time resolved gated images

(Δt=3 ns) at time delays of 130 ns and 250 ns for both single plasma (S_p) and colliding plasma (C_p) plumes for a mid-range laser energy (E_L) of ~300 mJ per seed plasma. The extended nature of the stagnation layer is evident throughout the emission lifetime of the plumes, demonstrating the unusual plume dynamics evident in stagnation layer formation.

B. Retarding field analyzer

A retarding field analyzer is composed of two parts. The first is the actual electrostatic detector, the venerable Faraday cup[36]. We employ an irregular internal geometry cup which is composed of a number of copper surfaces at various angles to the vertical plane. Such a configuration is proven to strongly mitigate secondary electron emission from the internal surface of the cup[37-39] and has been verified previously for the charge states of relevance here[40] (Cu^+ to Cu^{5+}) up to high kinetic energies[41] ($K_e \geq 40$ keV). Numerous RFA configurations have been developed for specialist applications such as large acceptance angle detectors[42], including a gridless type for ion temperature measurements[43], a Wien type filter analyzer for surface diagnostics[44] and cylindrical deflection type analyzers for low energy ion scattering[45]. The simplicity and robustness of a RFA has resulted in their proliferation in numerous areas of charge particle diagnostics such as semiconductors[46,47], electron beam detection[48-50], gaseous ion detection[51,52], heavy metal ion detection[53,54], high current discharge systems[55,56] and large volume plasma experiments including fusion studies[56-58].

Figure 1(d) presents a schematic of the gridded retarding field analyzer (RFA) and Faraday cup. A typical gridded RFA is composed of three parallel mesh covered apertures (of diameter ~8 mm in our case). The central grid/mesh is biased to various repeller voltages $+V_r$ while the outer two are grounded. This is usually followed by a secondary electron suppressor which can be another mesh or a ring, biased to a negative voltage larger than the cup bias. The three-grid system is placed in front of the Faraday cup and acts as a filter for incoming ions. The cup was made of a hollow copper cylinder, 50 mm in length and 15 mm in diameter with an 8 mm diameter entrance aperture and was biased to -600 V in this work. Although a secondary electron suppressor was fitted to our RFA (a charged ring), it was observed that even a relatively high bias on this ring (-1000 V) had no effect upon the recorded signal as the irregular internal geometry cup was able to compensate for secondary electron emission. A custom built linear ramping power supply (0-3 kV, 1.5 mA) provided the bias for the repeller grid. The ramp time on the supply was combined with the repetition rate of the laser to ensure a voltage step of ΔV_r=25 V between laser pulses. The mesh used was tungsten (plain weave mesh - 30% transmission, 20 μm wire diameter, 99.95% purity, nominal aperture 0.15 mm). The cup and mesh layers were separated by Teflon ring isolators, and housed in a Teflon cylinder positioned inside a grounded aluminium cylinder (see Fig. 1(d)).

A number of important design features must be included for successful operation of a gridded RFA. The maximum distance between the wires of the mesh must not significantly exceed the Debye length λ_D of the plasma. This is required to ensure a continuous sheath across the face of the mesh[59] and is particularly important for the repellor grid.

The primary challenge in gridded RFA operation is the competing requirements between the space-charge shielding of ions and electrons at the repeller versus the voltage required at the repeller grid[59]. For plasma plumes of sufficient density and kinetic energy space-charge shielding may result in insufficient penetration of the plume at the front of the repeller grid. This can result in the formation of a virtual charge emitting surface which changes the effective spacing between the grounded grids and the repeller and also the actual bias as experienced by the plasma[60]. This issue can be compounded by the requirement to ensure V_r is high enough to ensure sufficient electrostatic repulsive force ($\sim eV_r z_i$) at a particular ion kinetic energy (for charge state z_i). Distortion of the grid surface is also of concern as is heating due to intermittent current discharge.

One simple solution which strongly mitigates the above challenges is to employ a drift tube. The drift tube facilitates firstly time of flight (*TOF*) separation of each ion group and a concomitant drop in the plasma density. Secondly the lower plasma density also allows the repeller grid to be biased to relatively high values without arcing. The drop in plume density (which also increases the Debye length) helps to lessen the effects of space-charge shielding of the ions at the repellor[59] and also reduces the cumulative effects of electron and ion backscatter into the slower moving components within the plume[61]. We have utilized a d=1.13 m drift tube which allows the repeller grid bias to be set at values up to 1000 V for the entire fluence range used. No arcing was present and this maximum V_r bias was sufficient to repel all ion signals.

To diagnose the total charge yield (Q_{Total}) from each plasma, time dependent current traces for each detected ion charge state must be determined. This is achieved by recording the Faraday cup trace for a range of V_r bias values from 0 V to that bias which prevents all ions reaching the cup. Figure 2(a) presents Faraday cup traces for the entire fluence range used (with V_r =0 V) from a single seed plasma (S_p). Figure 2(b) displays the changing time dependent voltage trace produced by the cup for V_r=0 to +500 V for F=0.26 kJcm^{-2}. As V_r increases the repulsive electrostatic force of the repeller grid repels low energy ions for each charge state allowing the deconvolution point between the signals (or peaks) of each ion charge state to be observed. Figure 3(a) displays this procedure for Cu^+ to Cu^{5+} ions, plotting the total signal (V_r=0 V), the deconvolution points (⊕) for each ion group and the fitted deconvoluted current traces generated *via* the following shifted Maxwell-Boltzmann distribution equation[61,62]:

$$S(t) = Ct^{-4} \exp\left\{ \frac{-m}{2k_B T_s} \left(\frac{d}{t} - v_{CM} \right)^2 \right\} \quad \text{Eq. 4}$$

Where C is a normalization factor, m is the mass of the target atom (kg), k_B is Boltzmann constant (K), T_s is the kinetic temperature, d the time-of-flight distance (m) and v_{CM} is the centre-of-mass velocity (ms^{-1}) of the plasma plume (or ion groups). The exact procedure is as follows. The deconvolution points for Cu^+ (⊕ -grey) are overlaid with the total trace I_T. The portion of I_T to the right, and of amplitude less than the last deconvolution point for Cu^+ is extracted (all signal to the right of and lower than the grey horizontal line in Fig. 3(a)). Thus the deconvolution points for Cu^+ provide the rising edge of its current trace and the trailing edge is the portion of I_T

alluded to above. Only the peak region of the Cu^{+} current trace is thus absent. This data is used to generate the complete Cu^{+} current trace *via* Eq. 4 to produce I_{+}. This is then subtracted from I_T to produce the *residue* signal - R_1 (composed of the still combined Cu^{2+} to Cu^{5+} traces).

The above procedure is then repeated using the Cu^{2+} deconvolution points and remaining residue signal - R_1. The required portion of R_1 is combined with the Cu^{2+} deconvolution points and Eq. 4 is again used to generate the Cu^{2+} current trace. The residue signal - R_2 in this case is now composed of Cu^{3+} to Cu^{5+} signals. When the generated Cu^{4+} trace is finally subtracted from the last residue - R_4, this residue trace is the remaining Cu^{5+} signal. Summation of the generated Cu^{+} to Cu^{5+} traces should exactly match I_T. Here the match is almost perfect and the summed trace is obscured by the experimental trace. The individual current traces can be converted to a K_e distribution[54] *via* Eq. 5 and plotted against an energy axis given by Eq. 6.

$$f_z(E) = \frac{I_Z(t)t^3}{z_i emd^2} \qquad \text{Eq. 5}$$

$$E = \frac{1}{2}m\left(\frac{d}{t}\right)^2 \qquad \text{Eq. 6}$$

where I_z is the current trace of ionic state z_i, t is time (sec), e the electron charge, m is the mass of the atom (kg) and d is the drift tube (d=1.13 m). Figure 3(b) displays the K_e distribution for the S_p for F=0.26 $kJcm^{-2}$ extracted from current traces for Cu^{+} to Cu^{5+}. Charge yields can be calculated *via* integration of the time dependent current traces.

IV. RESULTS

Our results are divided into two sections. Firstly, using the technique outlined in section III, time dependent current traces are determined for all fluence values used for both single plasma (S_p) and colliding plasma plumes (C_p). From these traces charge resolved yields are obtained and compared in section IV.A. We also present the charge yield *(CYR)* parameter which we use to quantify the degree of enhancement (or attenuation) of charge yields from the C_p. In section IV.B kinetic energy distributions, calculated from time dependent current traces, are presented and discussed. Pronounced differences between the S_p and C_p are observed and are strongly charge dependent. These results strongly reinforce existing electrostatic charge integrated data[34,35] from C_p where both the peak and width of the kinetic energy distribution have been observed to be lowered in the colliding plasmas case.

A. Charge yield measurements

Figures 4(a) and (b) display the total charge yield (Q_{Total}) for each detected charge state over the fluence range employed for both the S_p and the C_p. In both cases the charge yield profile increases rapidly with fluence before displaying gradual convergence to a near-saturated condition at high fluence. The good separation of these curves and the relative values of Q_{Total} at or near saturation is in good agreement with results for all ion yields, from Cu^+ to Cu^{5+}, at near identical laser intensities (I_p~10^{10}-10^{11} Wcm^{-2}) from previous charge yield measurements using a conventional high voltage laser ion source[40,41].

The variation in total charge yield (Q_{Total}) with fluence (F) for the C_p were similar to those for the S_p, however near-saturation did not occur until slightly higher F values and the rising edge of the Q_{Total} profile at low F was more pronounced. This was observed for all charge states.

To quantify this difference and attempt to more thoroughly diagnose the effects of stagnation layer formation on relative ion yields we divided the charge yield from the C_p by twice that from the S_p. This parameter was termed the charge yield ratio *(CYR)* parameter. Where this parameter exceeds unity, stagnation layer formation results in superior charge yields from the C_p beyond simple summation of the charge yield from two single plumes. This data is presented in Table I.

It is clear from this table that this parameter exceeds unity for a discrete F range and the extent of that F range is charge dependent. The charge yield from the C_p should theoretically not exceed a value which is twice that of the S_p unless collisional processes within the stagnation layer (or during its early formation) lead to an increase in the average charge state and/or ion density.

To investigate this aspect of C_p the individual charge yields (Cu^+ to Cu^{5+}) were summed for each F value for both single and colliding plasmas. The value obtained, i.e., Q_{sum} also exhibited a rapid rise with fluence. This data is presented in Table II which also displays the charge summed *CYR* parameter. The following exponential function was fitted to the Q_{Sum} data:

$$Q_{Sum}(F) = A - (A - B)\exp(-(CF)^D) \quad \text{Eq. 7}$$

where *A, B, C* and *D* are constants (*C* and *D* are dimensionless) and *F* is the laser fluence ($kJcm^{-2}$). The values of *A* and B (in nC) shift the fitted base line and saturation level of the data while those within the exponent determine the increase in Q_{Sum} with *F*. These constants are presented in Table III for the C_p, S_p and $2xS_p$ summed charges (again assuming direct summation of the charge yield from two single plasma plumes). Using equation 7 the summed charge yields from each plasma configuration can be approximated by:

$$Q_{Sum}(F) \propto \exp((-2.75F^{-0.97})) \quad (S_p) \qquad \text{Eq. 8}$$

$$Q_{Sum}(F) \propto \exp((-3.65F^{-1.344})) \quad (C_p) \qquad \text{Eq. 9}$$

The constants presented in Table III for $2 \times S_p$ assume simple summation of the charge yield from an S_p. Thus it is appropriate that the constants *A* and *B* are approximately twice that for an S_p and that the rate of increase in the Q_{sum} profiles with fluence (represented here by *C* and *D*) are nearly identical to those from an S_p.

In considering the relative charge yields from the two plasma configurations, the quantitative difference could be significantly larger as the time-of-flight of the ions decreases. Three body recombination which strongly affects the charge yield close to the ablation surface results in a decreasing average charge state within the plasma plume. The recombination rate is proportional to $\approx z_i^3 N_e^2 T_e^{-9/2}$ where z_i is the charge state of the ion, N_e the electron density and T_e the electron temperature[63]. This

process determines the final ionic distributions in the early plasma plume. However it has been shown that after some critical distance[64] L_{CR}, the recombination rate begins to decrease strongly and is given by:

$$L_{CR} \cong \frac{T_{in}^{13/12} v_{ion}^{14/6} \tau^{13/6}}{N_c^{8/18} \phi^{8/6}} \qquad \text{Eq. 10}$$

T_{in} is the initial electron temperature (K) at the end of the laser pulse, v_{ion} is the ion velocity, τ is the laser pulse duration (s), N_c is the critical electron density (cm^{-3}) and ϕ is the spot diameter (m). The lowering of the recombination rate is related to the drop in plasma density as the plasma expands into the drift tube. As a result, 'freezing' of charge states should occur after this critical distance. Indeed L_{CR} values for laser plasma generation from laser pulses with λ=1.064 μm are typically on the order of a few centimetres[64].

It is also possible to reconstruct the charge yield at any particular distance (d) along the flight tube, for $d >> L_{CR}$, using analytically determined equations[65-67] which takes the form $Q \propto d^{-2}$. These relations can be used to compensate for dilution and expansion of the plume. Considering the above two aspects of laser plasma formation and expansion, it is highly probable that the *CYR* parameter for spatial scales less than L_{CR} could be significantly larger than those measured for here for d <1 m.

B. Kinetic energy distributions

Kinetic energy distributions were extracted from ion current traces *via* Eqs. 5 and 6. The width of the K_e profile at half maximum ($\Delta_{1/2}$) and the peak K_e for all

charge states and F values for both the S_p and C_p were obtained. This data is plotted in Fig. 5(a-f). The central trend observed for $\Delta_{1/2}$ and peak K_e was an increase in both with fluence which has been observed previously for both single and colliding plasma plumes. However there are some distinct differences between the absolute values of these peak and width parameters for these two cases, in their variation. In particular, for highly charged ions (e.g., the 5+ case) at high fluence values, both $\Delta_{1/2}$ and peak K_e are smaller in the C_p case compared to the S_p case. It is clear from figure 5 that the extent of this lowering of $\Delta_{1/2}$ and peak K_e and the location of the 'cross-over' point on the F scale (C_p value falling below the corresponding S_p value) is clearly dependent upon the charge state.

The $\Delta_{1/2}$ and peak K_e were also averaged for each charge state and plasma configuration. It can be seen from the resulting profiles, figures 6(a,b), that the transition from these values being greater for C_p than in the S_p in the charged averaged case is more abrupt, occurring at low F (~0.2 kJcm^{-2}) in comparison to the gradual reversal evident in the charge resolved yields (Figs. 5(a-f)). This highlights the need for charged resolved diagnostics of C_p dynamics if the dominant mechanisms which occur during stagnation layer formation are to be fully elucidated.

These results are in agreement with previous electrostatic (non-charged resolved) studies of colliding plasmas using angle resolved Faraday cup data for aluminium plasma plumes[31], and Langmuir probes for the study of various metals[32] (Al, Ti, Fe, Ni, Co Cu and Pt). In both reports the relevant detector was positioned beyond the recombination zone (L_{CR}) and employed approximately the same laser intensities as work reported here (I_p~10^{10}-10^{11} Wcm^{-2}). Faraday cup measurements[31]

of the $\Delta_{1/2}$ displayed the same cross over effect for the fluence range employed. $\Delta_{1/2}$ values for the C_p were larger than the equivalent S_p values, but only for low laser fluences. The largest reported difference was ~36 % at the maximum reported laser energy[31], where $\Delta_{1/2}$ (C_p) << $\Delta_{1/2}$ (S_p). The peak K_e from the C_p was larger than the calculated S_p value but only by a moderate percentage (~10%). However in that report, no aperture or filter control was employed to separate the seed plasmas from the stagnation layer and the results were not charged resolved.

Aperture control was employed in other work[32] which used Langmuir probes positioned at distances d= 38, 88 and 118 mm from a diaphragm aperture close to the plasma expansion axis (normal to the ablation surface). This blocked the majority of the plasma plume from the seed plasmas. The mean energy (ε_i) and maximum energy ($\varepsilon_{i.max}$) of the recorded plasma ions (assumed to be singly charged) were measured. For the colliding plasma data both ε_i and ε_{imax} were on average 50% lower than for the single plasma. In arriving at these values, these authors assumed that the average charge state was singly ionized. However, it is clear from our data that these values are lower in C_p compared to S_p only for the more highly charged ions and so their plasmas must have been on average more highly ionized than unity.

V. DISCUSSION

The total energy input (from the laser pulse) during C_p generation is exactly twice that for a S_p. The processes involved in stagnation layer formation for C_p dynamics must be inherently adiabatic. Conservation of energy principles thus require

some process to be enhanced at the expense of the recorded K_e distributions and this process must be charge dependent.

Laser generated plasma plumes exhibit strong internal magnetic and electric fields[68], which result in unique plume dynamics such as the phenomenon of plume splitting[69,70] which is attributed to electrostatic influences on ion/electron dynamics. Acceleration of positively charged particles is generally associated with the motion of fast electrons propagating away from the target surface[71] and such charge separation mechanisms[72] in laser plasma plumes originate from the hydrodynamic pressure gradient $F_p \sim \nabla P_e$ and the thermal force $F_t \sim \nabla T_e$. Electromagnetic influences within the plasma respond *via* the formation of dipole moments at the plasma front, resulting in electric fields outside the plasma plume and the generation of a non-isotropic internal electric field (which is orientated normal to the target surface). This internal field results in a shift in the measured ion energy distribution[73,74].

For very early phases in the plume history (during the laser pulse) fast electrons are ejected from the core of the plasma, establishing a positive charge at the target surface. This layer of fast electrons can separate from the combined ion and neutral cloud by up to one Debye length which can result in charge dependent acceleration of ions[74]. Measurements[74-80] of self-generated electric field intensities in laser generated plasma plumes for laser intensities of I_p=10^9-10^{19} Wcm^{-2} have shown that short lived electric fields, with values on the order of E_0~2×10^5-1.4×10^{12} Vcm^{-1}, are present. Although the exact nature and structure of dipole moments and the resulting space-charge forces within stagnation layers are not fully understood, it is reasonable to assume that such processes are certainly present within a stagnation

layer and could account for the observed results reported here. Indeed, given the strong charge dependency of our results, acceleration of ions by local, high gradient electric fields within the volume of the stagnation layer is highly probable.

If fast electrons stagnate before the heavy, slower ions, and highly charged ions stagnate earlier than less highly charged ions then prior electron layer stagnation could screen incoming ions for an extended time interval[31]. This would allow ions from opposing seed plumes to approach closely before space charge fields start to oppose this which would lead to a concomitant increase in the local electric field gradient. Direct measurements of electric fields[81-83] in or near the stagnation layer, compared to those detected from a single plasma plume, are necessary to gain a proper insight into the potential role of electric field effects on the stagnation layer dynamics if a full understanding of stagnation layer formation and the observed results for ion K_e distributions and ion charge yields is to be better understood.

CONCLUSION

We have performed a charge resolved electrostatic study for both colliding laser plasma and single plasma plumes using a retarding field analyzer (RFA) with a Faraday cup detector situated at the end of the drift tube. For a range of laser energies the ion yields for Cu^+ to Cu^{5+} was determined and compared. For a restricted range of fluences the total charge yield recorded from the C_p exceeds twice that from a S_p indicating a small but finite gain. The kinetic energy distributions clearly indicated a strong narrowing of the K_e profile and lowering of the peak K_e for C_p plumes. These effects were charge dependent and may suggest space-charge and ambipolar field

effects which result in strong ion acceleration in the presence of the stagnation layer as a significant influence. The resultant transfer of ion K_e to collisional ionization mechanisms enhances the charge yield from a colliding plasma stagnation layer. Future work will focus upon the charge yield and kinetic energies of colliding laser plasma plumes from metals for a range of atomic masses in the periodic table to explore possible scaling relations in the behaviour of stagnation layer formation.

Acknowledgements: The authors wish to acknowledge Enterprise Ireland (Grant No: SC/2003/0180), Science Foundation Ireland (Grant No. 07/IN.1/I1771) and the HEA PRTLI IV INSPIRE program of the Second National Development Plan program (NDP2) for financial support over the course of this project.

References:

[1]M. V. Babykin, E. K. Zavoiskii, L. I. Rudakov, V. A. Skoryupik (1963) Soviet Phys. [JETP] Vol. 16, pg. 1391.

[2]D. R. Bates, A. E. Kingston, R. W. P. McWhirter Proc. R. Soc., Lond. A267, 297 (1962).

[3]J. D. Jukes, J. Fluid Mech. Vol. 3, Iss. 3 (1957) pg. 275-285.

[4]D. W. Koopman, Physics Fluids, Vol. 15 (1972) pg. 1959-1969.

[5] P. T. Rumsby, J. W. M. Paul, M. M. Masoud, Plasma Phys. Control. Fusion Vol. 16 (1974) pg. 969.

[6]A. R. Bell, P. Choi, A. E. Dangor, O. Willi, D. A. Bassett, C. J. Hooker, Physical Review A 38 (1988) pg. 1363-1369.

[7]A. S. Wan, T. W. Barbee, Jr., R. Cauble, P. Celliers, L. B. Da Silva, J. C. Moreno, P. W. Rambo, G. F. Stone, J. E. Trebes, F. Weber, Phys. Rev. E, 55, 6293 (1997).

[8]K. A. Brueckner, S. Jorna, Laser-driven fusion, Reviews of Modern Physics. Vol. 46 (1974) pg. 325-367.

[9]N. C. Woolsey, Y. A. Ali, R. G. Evans, R. A. D. Grundy, S. J. Pestehe, P. G. Carolan, N. J. Conway, R. O. Dendy, P. Helander, K. G. McClements, J. G. Kirk, P. A. Norreys, M. M. Notley, S. J. Rose, Phys of Plasmas, Vol. 8 (2001) pg. 2439-2445.

[10]B. A. Remington, S. W. Haan, S. G. Glendinning, J. D. Kilkenny, D. H. Munro, R. J. Wallace, Phys. Fluids B, 4**,** 4, (1992) pg. 967-978.

[11]A. A. Gorbunov , W. Pompe, A. Sewing, S. V. Gaponov, A. D. Akhsakhalyan, I. G. Zabrodin, I. A. Kas'kov, E. B. Klyenkov, A. P. Morozov, N. N. Salaschenko, R. Dietsch, H. Mai, S. Viillmar. Appl. Surf. Sci, 96-98 (1996) 649-655.

[12]A.A. Gorbunov, W. Pompe, A. Sewing, S.V. Gaponov, A.D. Akhsakhalyan, I.G. Zabrodin, I.A. Kas'kov, E.B. Klyenkov, A.P. Morozov, N.N. Salaschenko, R. Dietsch, H. Mai, S. Völlmar, Appl. Surf. Sci. 96-98 (1996) 649-655.

[13]E.V. Pechen. S.1. Krasnosvobodtsev, G. Kessler, A. Richter, M. Panzner. 0. Grossman, A. Teresiak, Phys. Status Solidi (a) 131 (1992) 179.

[14]M. D. Strikovsky, E. B. Klyuenkov, S. V. Gaponov, I. Schubert, C. A. Copetti, Appl. Phys. Lett. Vol. 63 (1993) pg. 1146-1148.

[15]S. S. Harilal, C. V. Bindhu, H.-J. Kunze, J. Appl. Phys, 89 (2001) pg. 4737-4740.

[16]F. Ruhl, L. Ascke, H.-J. Kunze, Physics Letts. A 225 (1997) 107-112.

[17]C. Chenais-Popovics, O. Rancu, P. Renaudin, H. Kawagoshi, J. C. Gauthier, M. Dirksmoller, I. Uschmann, T. Missalla, E. Forster, O. Renner, E. Krousky, H. Pepin,

O. Larroche, O. Peyrusse, J. Quant. Spectrosc. Radiat. Transfer. Vol, 54, No. 1/2, pg. 105-112, 1995.

[18]T. Atwee, H-J. Kunze, J. Phys. D: Appl. Phys. 35 (2002) pg. 524-528.

[19]Bosch R A, Berger R L, Failor B H, Charatis G, Kauffman R L 1992 Phys. Fluids B 4, 979.

[20]Atwee T, Harilal S. S, Kunze H-J. J. Phys. D: Appl. Phys. 34 (2001) pg. 1213-1218.

[21]C. Chenais-Popovics, P. Renaudin, O. Rancu, F. Gilleron, J.-C. Gauthier, O. Larroche, O. Peyrusse, M. Dirksmöller, P. Sondhauss, T. Missalla, I. Uschmann, E. Förster, O. Renner, E. Krouský, Physics of Plasmas, Vol. 4 (1997) pg.190-208.

[22]R. Fabbro, B. Faral, J.C. Gauthier, C. Chenais-Popovics, J.P. Geindre, H. Pepin, Laser and Particle Beams, 8 (1990) 73-79.

[23]O.Rancu, P. Renaudin, C. Chenais-Popovics, H. Kawagashi, J. C.Gauthier, M. Dirksmöller, T. Missalla, I. Uschmann, E. Förster, O. Larroche, O. Peyrusse, O. Renner, E. Krouský, H. Pépin, T. Shepard, Physical Review Letters 75 (1995) 3854-3857.

[24]Purvis M, Grava J, Filevich J, Marconi M C, Dunn J, Moon S J, Shlyaptsev V. N., Jankowska E, Rocca J. J., 2007 Phys. Rev. E 76 046402.

[25]Smith R A, Lazarus L, Hohenberger M, Moore A S, Robinson J S, Gumbrell E. T., Dunne M., 2007 Astrophys. Space Sci. 307, 131.

[26]S. M. Pollaine, R. L. Berger, C. J. Keane, Phys. Fluids B 4(4) (1992) pg. 989-991.

[27]P. W. Rambo, J. Denavit, Journal of Computational Physics 98 (1992) pg. 317-331.

[28]E. Leboucher-Dalimier, P. Angelo, P. Gauthier, P. Sauvant, A. Poquerusse, H. Derfoul, T. Ceccotti, C. A. Back, T. D. Shepard, E. Forster, I. Uschmann, M. Vollbrecht. J. Quant. Spectrosc. Radiat. Transfer. Vol, 58, No. 4-6, pg. 721-735, 1997.

[29]C. Sánchez-Aké, D. Mustri-Trejo, T. García-Fernández, M. Villagrán-Muniz, Spectrochimica Acta Part B 65 (2010) 401-408.

[30]J. Dardis, J. T. Costello, Spectrochimica Acta Part B 65 (2010) pg. 627-635.

[31]P. Hough , C. McLoughin , T. J. Kelly, P. Hayden , S. S. Harilal , J. P. Mosnier, J. T. Costello, J. Phys. D: Appl. Phys. 42 (2009) 055211.

[32]E. Camps, L. Escobar-Alarcon, E. Haro-Poniatowski, M. Fernandez-Guasto. Appl. Surf. Sci. 197-198 (2002) 239-245.

[33]H. Luna, K. D. Kavanagh, J. T. Costello. J. Appl. Phys. Vol. 101**,** 033302 (2007).

[34]A. Tselev, A. Gorbunov, W. Pompe. Appl. Phys. A 69, 353-358 (1999).

[35]P. Hough, C. Fallon, C. McLoughin, P. Yeates, T. J. Kelly, P. Hayden, J. P. Mosnier, E. T. Kennedy, S. S. Harilal, J. T. Costello. (Submitted May 2011 – Under Review, Journal of Physics D: Applied Physics).

[36]J. S. Pearlman, Rev. Sci. Instrum. Vol. 48 (1977) pg. 1064-1067.

[37]J. F. Seamans, W. D. Kimure, Rev. Sci. Instrum. Vol. 64 (1993) pg. 460-469.

[38]H. Chuaqui, M. Favre, E. Wyndham, L. Arroyo, P. Choi, Rev. Sci. Instrum. Vol. 60, (1989) pg. 141-142.

[39]T. Iida, R. Taniguchi, T. Fujimoto, K. Sumita, Rev. Sci. Instrum. Vol. 53 (1982) pg. 168-170.

[40]P. Yeates, J. T. Costello, E. T. Kennedy, Rev. Sci. Instrum, Vol. 81, 043305 (2010).

[41]P. Yeates, J. T. Costello, E. T. Kennedy, Plasma Sources Sci. Technol. 19 (2010) 065007 (13pp).

[42]A. W. Molvik, Rev. Sci. Instrum. Vol. 52 (1981) pg. 704-711.

[43]S. Falabella and A. W. Molvik, Rev. Sci. Instrum. Vol. 61 (1990) pg. 1892-1899.

[44]Y. Sakai, M. Kato, S. Masuda, Y. Harada, T. Ichinokawa, Surf. Rev. Lett. 5, 1199 (1998).

[45]N. Bundaleski, Nucl. Instrum. Methods Phys. Res. B 198, 208 (2002).

[46]Y. Franghiadakis, C. Fotakis, P. Tzanetakis, Appl. Phys. A 68, 391-397 (1999).

[47]Y. Franghiadakis, C. Fotakis, P. Tzanetakis, J. Appl. Phys. Vol. 84 (1998) pg. 1090-1094 .

[48]Y. Cui, Y. Zou, A. Valfells, M. Reiser, M. Walter, I. Haber, R. A. Kishek, Rev. Sci. Instrum. Vol. 75 (2004) pg. 2736-2745.

[49]J. Lohr, Rev. Sci. Instrum. Vol. 45 (1974) pg. 1168-1169.

[50]S. Stephanankis, W. Bennett, Rev. Sci. Instrum. Vol. 39 (1968) pg. 1714-1721.

[51]J. E. Robinson, J. F. Clarke, Rev. Sci. Instrum. Vol. 42 (1971) pg. 434-437.

[52]A. Misra, T. Srivastava, R. K. Thareja. International Journal of Modern Physics B. Vol. 13, No. 2 (1999) pg. 1503-1512.

[53]A. Rupp, K. Rohr, J. Phys. D: Appl. Phys. 28 (1995) pg. 68-472.

[54]F. Belloni, D. Doria, A. Lorusso, V. Nassisi, Rev. Sci. Instrum, Vol. 75 (2004) pg. 4763-4768.

[55]C. Rustenberg, M. Lindmayer, B. Jutter, H. Pursch. IEEE Trans. Plasma. Sci. Vol. 23 (1995) pg. 909-914.

[56]A. W. Molvik, Rev. Sci. Instrum. Vol. 52 (1981) pg. 704-711.

[57]T. Honzawa, T. Sekizawa, Y. Miyauchi, T. Nagasawa, Jpn. J. Appl. Phys. Vol. 32 (1993) pg. 5748-5753.

[58]T. Baloniak, R. Reuter, C. Flotgen, A. Von Keudell. J. Phys. D: Appl. Phys. 43 (2010) 055203.

[59]R. Jones, Rev. Sci. Instrum. Vol .49 (1978) pg. 21-23.

[60]J. Chang, D. W. Swain, L. P. Mix, J. Appl. Phys. Vol. 44 (1973) pg. 2113-2114.

[61]R. K. Dwivedi, S. P. Singh, R. K. Thareja, Int. J. Mod. Phys. B12, 2619 (1998).

[62] R. K. Dwivedi, S. P. Singh and R. K. Thareja, Int. J. Mod. Phys. B12, 2619 (1998).

[63]J. Krasa, A. Lorusso, D. Doria, F. Belloni, V. Nassisi, K. Rohlena, J. Phys. D: Appl. Phys. 39 (2006) pg. 294-300.

[64]I. V. Roudskoy, Laser Part. Beams Vol. 14 (1996) pg. 369.

[65]J. Krasa, L. Laska, K. Rohlena, M. Pfeifer, J. Skala, B. Kralikova, P. Straka, Appl. Phys. Letts, Vol. 75 (1999) pg. 2539.

[66]J. Krasa, A. Lorusso, D. Doria, F. Belloni, V. Nassisi, K. Rohlena, Plasma Phys. Control. Fusion, Vol. 47 (2005) pg. 1339-1349.

[67]E. Woryna, J. Wolowski, B. Králiková, J. Krasa, L. Laska, M. Pfeifer, K. Rohlena, J. Skala, V. Perina, F. P. Boody, R. Höpfl, H. Hora, Vol. 71 (2000) pg**.** 949-951.

[68]Isak. I. Beilis, Laser Part. Beams, 25, (2007) pg. 53.

[69]J. Wild, P. Kudra, T. Gronych, T. Jirsak, P. Kubat, Z. K. Zelinger, S. Civis, Czech J. Phys, Vol 53, No 2, Feb, (2003).

[70]N. M. Bulgakova, A. V. Bulgakov, O. F. Bobrenok, Phys. Rev. E 62, 5624 (2000).

[71]N. M. Bulgakova, A. V. Bulgakov, O. F. Bobrenok, Phys. Rev. E 62, 5624 (2000).

[72]M. Borghes, D. H. Campbell, A. Schiavi, M. G. Haines, O. Willi, A. J. MacKinnon, P. Patel, L. A.Gizzi, M. Galimberti, R. J. Clarke, F. Pegoraro, H. Ruhl, S. Bulanov, Physcics of Plasmas, Vol 9, (2002) pg. 2214-2220.

[73]J. A. Stamper, Laser Part. Beams 9, (1991) pg. 841.

[74]L. Torrisi, S. Gammino, L. Laska, J. Krasa, K. Rohlena, J. Wolowski, Czech J. Phys. Vol. 56 (2006), Suppl B. B580-B586.

[75]M. Borghesi, S. Kar, L. Romagnani, T. Toncian, P. Antici, P. Audebert, E. Brambrink, F. CecchErini, C. A. Cecchetti, J. Fuchs, M. Galimberti, L. A. Gizzi, T. Grismayer, T. Lyseikina, R. Jung, A. Machhi, P. Mora, J. Osterholtz, A. Schiavi, and O. Willi, Laser Part. Beams, *25* (2007) pg. 161.

[76]N.C. Woolsey, J. Howe, D.M. Chambers, C. Courtois , E. Forster, C. D. Gregory, I. M. Hall, O. Renner, I. Uschmann, High Density Physics 3 (2007) pg. 292-296.

[77]M. Roth, A. Blazevic, M. Geissel, T. Schlegel, T. E. Cowan, M. Allen, J. - C. Gauthier, P. Audebert, J. Fuchs, Phys. Rev. Special topics - Accelerators and Beams, Vol 5, 061301 (2002).

[78]J. N. Olsen, C. W. Mendel Jr, J. Appl. Phys, Vol. 46 (1975) pg. 4407-4415.

[79]L. Torrisi, S. Gammino, Rev. Sci. Instrum. Vol. 77, 03B707 (2006).

[80]L. Torrisi, D. Mascali, R. Miracoli, S. Gammino, N. Gambino, L. Giuffrida, D. Margarone. J. Appl. Phys. Vol. 107, 123303 (2010).

[81]A. V. Kabashin, P. I. Nikitin, W. Maine, M. Sentis, Appl. Phys. Letts, Vol. 71 (1998) pg. 25-27.

[82]A. V. Kabashin, P. I. Nikitin, Quantum Electron. 27, 536 (1997).

[83]A. I. Barchukov, V. I. Konov, P. I. Nikitin, A. M. Prokhorov, Zh. Eksp. Teor. Fiz. 78, 957 (1979) [Sov. Phys. JETP 51, 482 (1980)].

TABLE I. *CYR* parameter for all detected ions. Fluence (column 1), charge yield ratio for Cu^{+} to Cu^{5+} (columns 2-5).

F **(kJcm^{-2})**	Cu^{+}	Cu^{2+}	Cu^{3+}	Cu^{4+}	Cu^{5+}
0.08	**0.63**	**0.52**	**0.56**	**0.73**	**------**
0.11	**0.79**	**0.71**	**0.70**	**0.90**	**------**
0.15	**1.02**	**0.83**	**0.89**	**1.02**	**0.44**
0.26	**1.17**	**0.97**	**1.02**	**1.08**	**0.65**
0.40	**1.27**	**1.03**	**1.09**	**1.10**	**0.97**
0.56	**1.32**	**1.09**	**1.07**	**1.07**	**1.18**
0.71	**1.33**	**1.02**	**0.99**	**0.97**	**1.21**
0.84	**1.22**	**0.88**	**0.85**	**0.86**	**0.95**

TABLE II. Fluence (column 1), total charge summation (Q_{sum}) for each seed plasma (column 2) and colliding plasmas (column 3) and summed charge *CYR* parameter (column 4). This data was obtained *via* summation of the individual ionic charge yields displayed in Fig. 4(a).

F (kJcm^{-2})	Q_{Sum} (nC) - S_p	Q_{Sum} (nC) - C_p	*CYR (Charge Summed)*
0.08	1.82	2.07	0.56
0.11	4.42	6.58	0.74
0.15	6.92	12.15	0.87
0.26	8.87	18.05	1.03
0.40	10.39	22.77	1.09
0.56	12.39	28.08	1.13
0.71	13.75	29.59	1.08
0.84	14.41	26.99	0.94

TABLE III. Constants for Eq. 7 fitted to the total charge summation data in Table I for the colliding plasma (C_p), the single plasma (S_p) and twice the S_p.

Target	A(nC)	B(nC)	C	D
S_p	16.07	0.18	2.75	0.97
$2\times S_p$	32.20	0.30	2.77	0.95
C_p	28.10	0.42	3.65	1.34

FIG. 1 (a) (Colour online) Schematic of the experimental system. (b) Optical and target configuration. The laser beam was separated *via* a wedge prism and the two beams were focused onto the planar copper target using a 22 cm convex-plano lens. (c) The retarding field analyzer (RFA). (d) Time gated images (Δt=3 ns) of a single plasma plume (S_p) and colliding (C_p) Typical laser plasmas plumes for time indices t=130 and 250 ns for copper planar targets (single and colliding plasmas).

FIG. 2 (a) (Colour online) Total Faraday cup signals versus fluence (F) from the single plasma (S_p). In this case the cup was biased to -500 V while the repeller grid bias V_r was 0 V. (b) Faraday cup signals for the single plasma (F=0.26 kJcm^{-2}) with V_r varying from 0 to +500 V. The approximate locations of the peaks of Cu^+ to Cu^{5+} are labelled. These peaks shift along the temporal axis as low energy ions for each charge state are increasingly rejected by increasing electrostatic repulsion at the repeller grid.

FIG. 3 (a) (Colour online) Deconvoluted current traces for Cu^+ to Cu^{5+} for the single plasma (S_p) at F=0.26 kJcm^{-2}. The crossed circular labels are the deconvolution points between each time dependent current peak observed in Fig. 2(b) as V_r increases. (b) Kinetic energy (K_e) distribution for Cu^+ to Cu^{5+} using Eq. 4 to convert time dependent current traces.

FIG. 4 (Colour online) Total charge yield (Q_{Total}) versus fluence (F) for the single plasma (a) and colliding plasma (b) for detected charge states Cu^+ to Cu^{5+}. These are calculated by integrating the time dependent current traces in Fig. 3(a).

FIG. 5 (a-c) (Colour online) Kinetic energy (K_e) profile width at half maximum (PWHM) for Cu^{+}, Cu^{3+} and Cu^{5+} versus fluence (F). As the charge state and fluence increase the $\Delta_{1/2}$ and peak K_e decrease strongly for the C_p. (d-f) K_e peak versus F for Cu^{+}, Cu^{3+} and Cu^{5+}. The F dependent profiles for K_e and $\Delta_{1/2}$ both demonstrate a transitional relationship as the charge state increases (for a fixed fluence). However for Cu^{3+} peak K_e measurements (e) the transition occurs across the studied F range. This was also observed for Cu^{2+} and $Cu^{4+}\Delta_{1/2}$ and peak K_e measurements (not shown here).

FIG. 6 (a) (Colour online) Averaged profile width at half maximum ($\Delta_{1/2}$) and (b) averaged peak kinetic energy (K_e) for both the S_P and the C_p versus fluence (F).

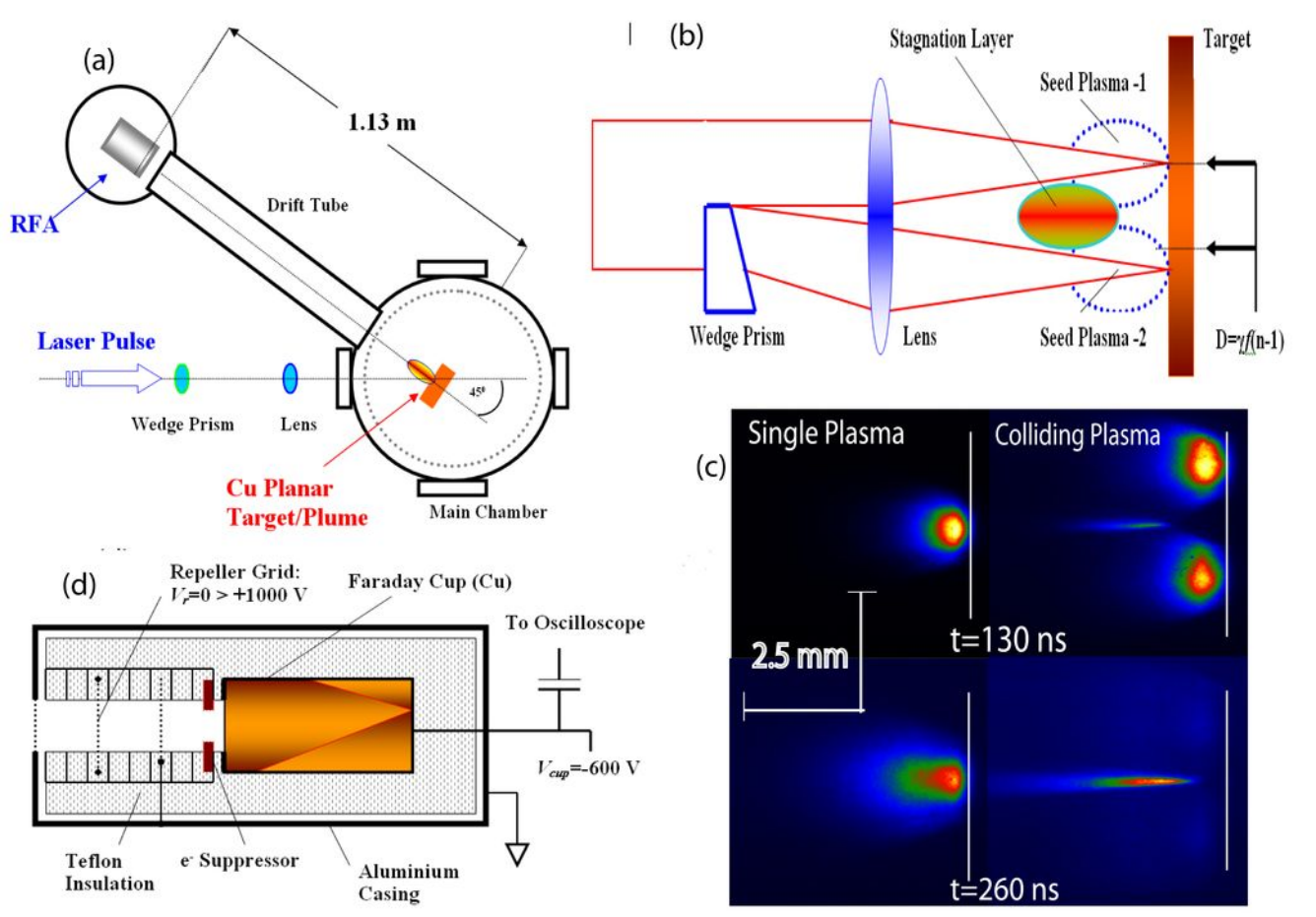
(a)
1.13 m
RFA
Drift Tube
Laser Pulse
Wedge Prism
Lens
45°
Cu Planar
Target/Plume
Main Chamber
(b)
Stagnation Layer
Target
Seed Plasma -1
Wedge Prism
Lens
Seed Plasma -2
D=yf(n-1)
(c)
Single Plasma
Colliding Plasma
2.5 mm
t=130 ns
t=260 ns
(d)
Repeller Grid:
Vr=0 > +1000 V
Faraday Cup (Cu)
To Oscilloscope
Vcup=-600 V
Teflon
Insulation
e- Suppressor
Aluminium
Casing

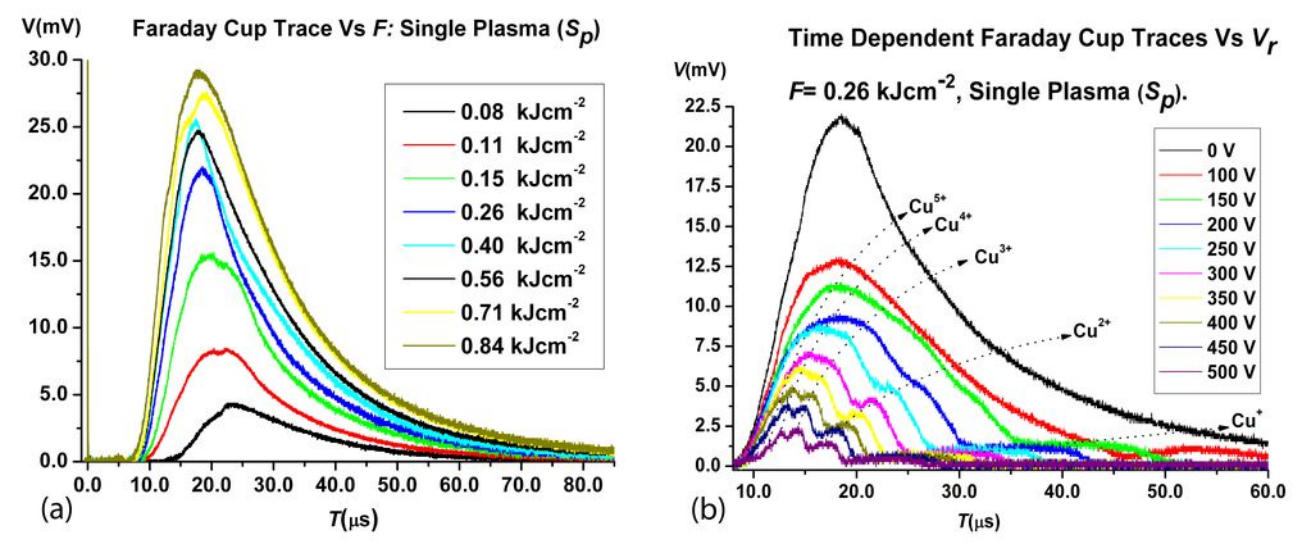
V(mV)
Faraday Cup Trace Vs F: Single Plasma (Sp)
30.0
25.0
20.0
15.0
10.0
5.0
0.0
0.0
10.0
20.0
30.0
40.0
50.0
60.0
70.0
80.0
T(μs)
(a)
0.08 kJcm-2
0.11 kJcm-2
0.15 kJcm-2
0.26 kJcm-2
0.40 kJcm-2
0.56 kJcm-2
0.71 kJcm-2
0.84 kJcm-2
Time Dependent Faraday Cup Traces Vs Vr
V(mV)
F= 0.26 kJcm-2, Single Plasma (Sp).
22.5
20.0
17.5
15.0
12.5
10.0
7.5
5.0
2.5
0.0
10.0
20.0
30.0
40.0
50.0
60.0
T(μs)
(b)
Cu5+
Cu4+
Cu3+
Cu2+
Cu+
0 V
100 V
150 V
200 V
250 V
300 V
350 V
400 V
450 V
500 V

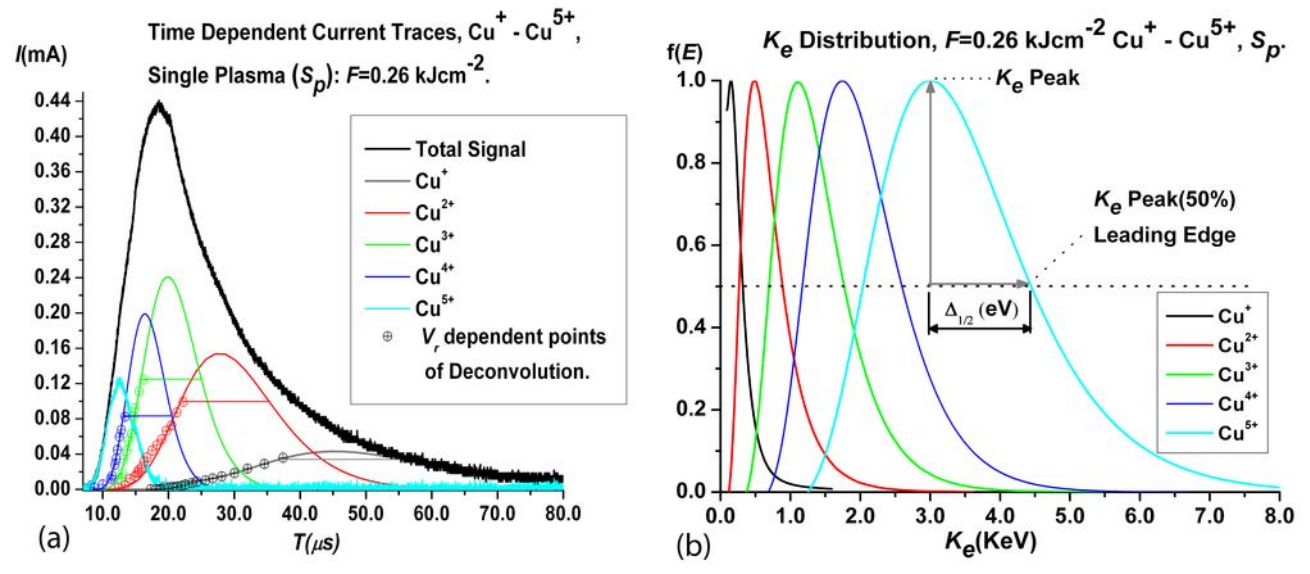
Time Dependent Current Traces, Cu+ - Cu5+,
Single Plasma (Sp): F=0.26 kJcm-2.
I(mA)
0.44
0.40
0.36
0.32
0.28
0.24
0.20
0.16
0.12
0.08
0.04
0.00
10.0
20.0
30.0
40.0
50.0
60.0
70.0
80.0
T(μs)
(a)
Total Signal
Cu+
Cu2+
Cu3+
Cu4+
Cu5+
Vr dependent points
of Deconvolution.
Ke Distribution, F=0.26 kJcm-2 Cu+ - Cu5+, Sp.
f(E)
1.0
0.8
0.6
0.4
0.2
0.0
Ke Peak
Ke Peak(50%)
Leading Edge
Δ1/2 (eV)
0.0
1.0
2.0
3.0
4.0
5.0
6.0
7.0
8.0
Ke(KeV)
(b)
Cu+
Cu2+
Cu3+
Cu4+
Cu5+

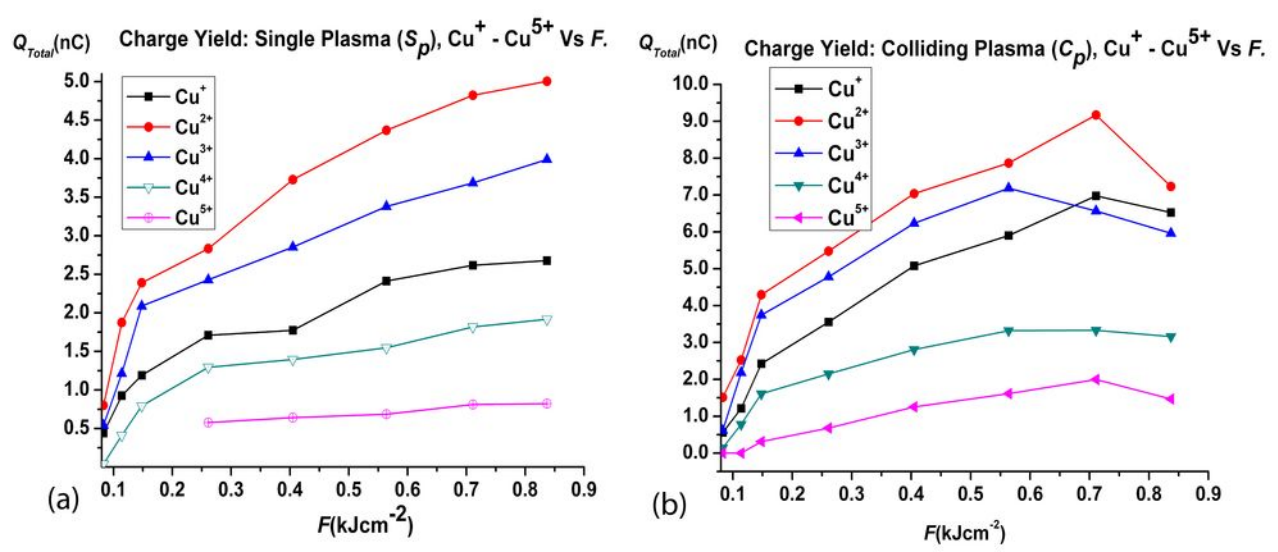
Q_{Total}(nC)
Charge Yield: Single Plasma (S_p), Cu^+ - Cu^{5+} Vs F.
Cu^+
Cu^{2+}
Cu^{3+}
Cu^{4+}
Cu^{5+}
5.0
4.5
4.0
3.5
3.0
2.5
2.0
1.5
1.0
0.5
0.1
0.2
0.3
0.4
0.5
0.6
0.7
0.8
0.9
F(kJcm^{-2})
(a)
Q_{Total}(nC)
Charge Yield: Colliding Plasma (C_p), Cu^+ - Cu^{5+} Vs F.
Cu^+
Cu^{2+}
Cu^{3+}
Cu^{4+}
Cu^{5+}
10.0
9.0
8.0
7.0
6.0
5.0
4.0
3.0
2.0
1.0
0.0
0.1
0.2
0.3
0.4
0.5
0.6
0.7
0.8
0.9
F(kJcm^{-2})
(b)

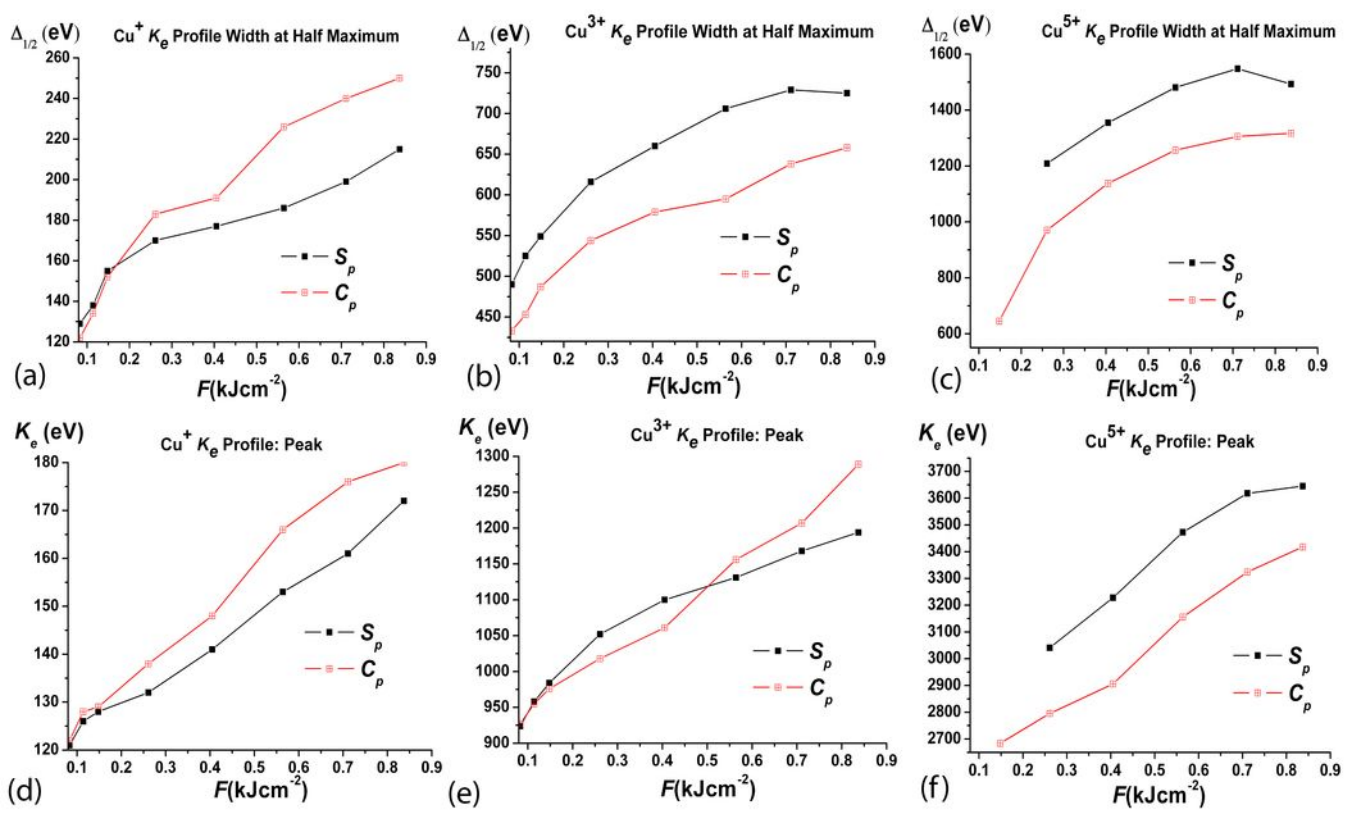
Δ1/2 (eV)
Cu+ Ke Profile Width at Half Maximum
Sp
Cp
(a)
F(kJcm-2)
Δ1/2 (eV)
Cu3+ Ke Profile Width at Half Maximum
Sp
Cp
(b)
F(kJcm-2)
Δ1/2 (eV)
Cu5+ Ke Profile Width at Half Maximum
Sp
Cp
(c)
F(kJcm-2)
Ke (eV)
Cu+ Ke Profile: Peak
Sp
Cp
(d)
F(kJcm-2)
Ke (eV)
Cu3+ Ke Profile: Peak
Sp
Cp
(e)
F(kJcm-2)
Ke (eV)
Cu5+ Ke Profile: Peak
Sp
Cp
(f)
F(kJcm-2)

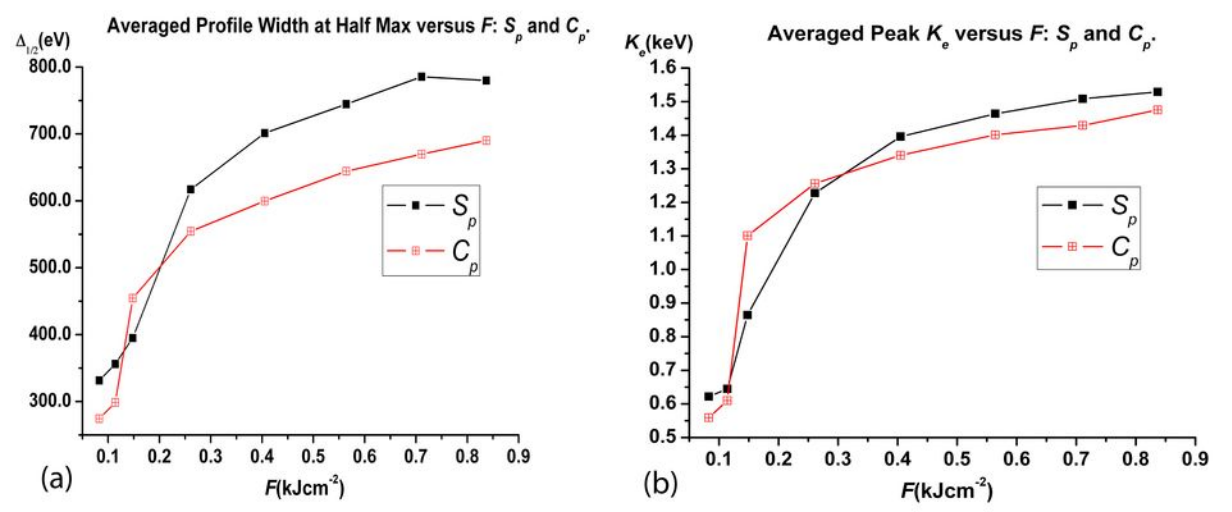
Averaged Profile Width at Half Max versus F: Sp and Cp.
Δ1/2(eV)
800.0
700.0
600.0
500.0
400.0
300.0
Sp
Cp
0.1
0.2
0.3
0.4
0.5
0.6
0.7
0.8
0.9
F(kJcm-2)
(a)
Averaged Peak Ke versus F: Sp and Cp.
Ke(keV)
1.6
1.5
1.4
1.3
1.2
1.1
1.0
0.9
0.8
0.7
0.6
0.5
Sp
Cp
0.1
0.2
0.3
0.4
0.5
0.6
0.7
0.8
0.9
F(kJcm-2)
(b)